ADVANCED MATERIALS INTERFACES
Open Access
www.advmatinterfaces.de

Mussel-Inspired Polyglycerol Coatings for Surface Modification with Tunable Architecture

Peng Tang, Guoxin Ma, Philip Nickl, Chuanxiong Nie, Leixiao Yu, and Rainer Haag**

Mussel-inspired coatings, known for their outstanding substrate-independent adhesive capabilities, have numerous potential applications in materials science and biomedical fields. To improve the understanding of how these polymers' molecular structure and chemical composition affect their coating mechanisms and resulting coating properties, herein three mussel-inspired polymers are developed: dendritic polyglycerol with 40% catechol groups and 60% amines (dPG40), linear polyglycerol with 80% catechols and 20% amines (lPG80), and finally lPG40 with 40% catechols and 60% amines. After a series of characterizations, it is found that chemical surface modification with a monolayer coating can be easily achieved with lPG40, and that robust and well-defined nano- to micro-structural surface coatings are possible with lPG80 and dPG40. Tunable properties are found to include not only coating speed, but coating thickness, roughness, and surficial topography. This diverse suite of controllable attributes enables mussel-inspired polyglycerol (MiPG) coatings to satisfy a wide-range of applications on multiple materials.

1. Introduction

In the past decades, many surface modification techniques, including chemical vapor deposition (CAD),[1] self-assembly of monolayer coating (SAM),[2] spin-coating,[3] surface grafting to/from chemistry,[4] have been developed and successfully used to endow materials with different chemical, physical and biological properties to extend their application.[5] Compared to traditional chemical modification, increasing evidence suggests that the construction of well-defined nanostructures and/or microstructures on the surface of biomaterials and biomedical devices, such as dental implants,[6] orthopaedic implants,[7] and artificial hips,[8] can play a vital role in regulating cell activities and functions, particularly in the domain of tissue engineering. The native extracellular matrix (ECM) is a macromolecular network complex that possesses a microscale and nanoscale hierarchical structure to mediate many aspects of cell behavior including cell adhesion, growth, proliferation, differentiation, and immune response.[9] In that sense, ECM-mimicking biomaterials with nanostructural or microstructural surfaces are exceptionally appealing in cellular studies. Hou et al. engineered hydrogels with different stiffness and roughness to investigate the cellular mechano-response of stem cells and induce osteogenesis of MSC.[10] Evidence shows that the tailored nano-structural surface coatings can also greatly enhance the capture efficiency of biochips toward circulating cancer cells.[11] Clinically, micro- to nanoscale topographies on dental implants were extensively used to improve osseointegration.[6] Therefore, versatile methods, e.g. stereolithography (SLA),[12,13] chemical etching,[14] electrospinning,[15] and polymer coatings,[16] were developed to engineer various micro/nano-structures, including nanorods,[17] nanopillars,[18] and nanofibers,[19] to meet the requirements of different applications. However, SLA and chemical etching face the problems of multiple-step processes and strict conditions. Moreover, most polymer coatings require reactive moieties between the biomedical devices and polymers, limiting both the choice and applications of biomaterials use. Developing a method that is simple and substrate-independent is therefore especially intriguing and promising.

Benefiting from the abundant amine groups (lysine) and catechol groups (3,4-dihydroxyl-L-phenylalanine, in the mussel foot proteins (mfps, e.g. 15% mol% for mfps-1 and 28% mol% for mpfs-5[20]), mussels can adhere and quickly form strong surface-adherent protein films on virtually any material's surface through their mfp-rich byssus.[21] Dopamine, containing both the catechol and amino groups, was used as the first generation of mussel-inspired building blocks for surface coating. The resulting polydopamine (PDA) films were found capable of adhering to almost all kinds of solid surfaces.[22] However, the coating process took up to tens of hours to achieve a very thin PDA layer (≈50 nm

P. Tang, G. Ma, P. Nickl, C. Nie, R. Haag
Institute for Chemistry and Biochemistry
Freie Universität Berlin
Takustraße 3, 14195 Berlin, Germany
E-mail: haag@chemie.fu-berlin.de
L. Yu
State Key Laboratory of Oral Diseases
West China Hospital of Stomatology
Sichuan University
Chengdu, Sichuan 610041, China
E-mail: leixiaoyu@scu.edu.cn

The ORCID identification number(s) for the author(s) of this article can be found under https://doi.org/10.1002/admi.202300165

DOI: 10.1002/admi.202300165

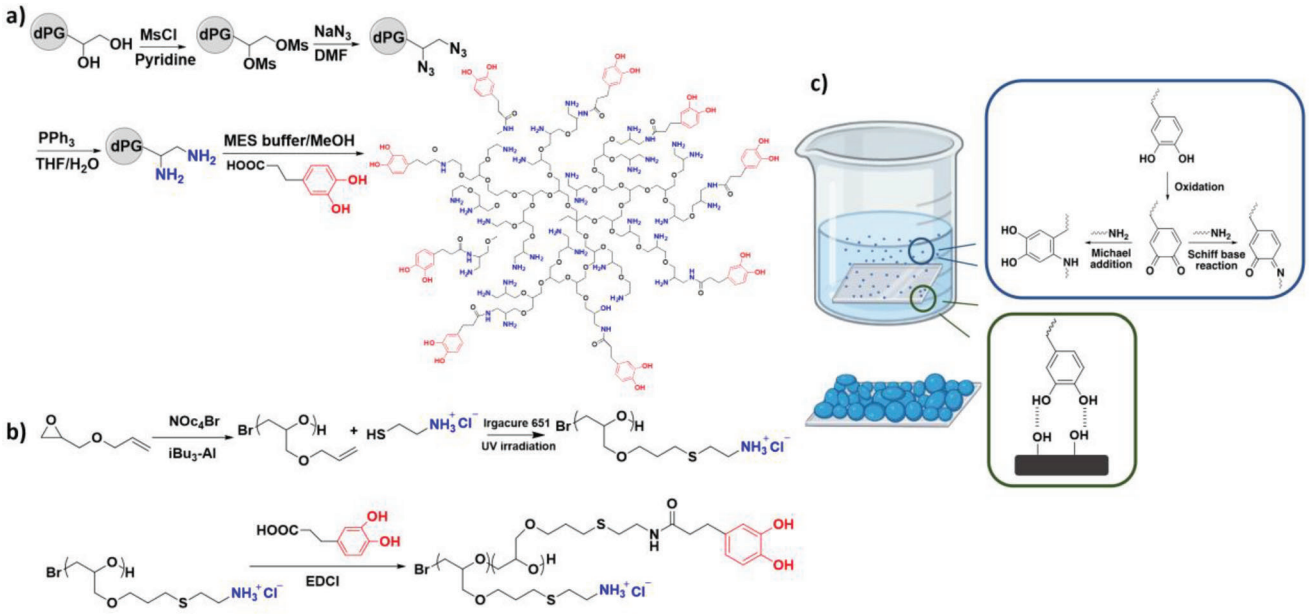

Figure 1. Mussel-inspired polyglycerol polymers. a) Structure of dPG40 with 40% catechol and 60% amino groups. b) Structure of catecholic lPG polymers. c) MiPG coating is achieved by dip-coating method under basic conditions. Polymer aggregates adsorb to substrates and bond tightly via hydrogen bond (with glass substrates). Possible reactions involved in the process of MiPG coating are indicated in the box.

in thickness) with limited surface structures. To accelerate the self-polymerization of dopamine, many methods, for example oxidants,[23] catalysts,[24] UV irradiation,[25] and microwave,[22] were used to promote the involved reaction kinetics including Michael addition, Schiff base reaction, and oxidative coupling.[26] In spite of improved coating processes, it is still hard to obtain well-defined surface structures, especially microstructures via polydopamine coatings. Mimicking the molecular structure of mussel foot proteins, we previously developed several hetero-multivalent catecholic polymers.[11,16] Many coatings and surficial structures have been thereby achieved through those building blocks. However, the relationship between the polymeric molecular structures and the resulting nano-/microscale coating structures had not yet been fully understood, which is essential for the design of coating polymers and fabrication of topographical structures.

Herein, three MiPGs with different polymer conformation and catechol functionality, i.e., mussel-inspired dendritic polyglycerol with 40% catechol groups (dPG40), and mussel-inspired linear polyglycerol with 80% and 40% of catechol groups (lPG80 and lPG40) were synthesized to understand the underlying reaction processes and establish relationship between the molecular structure and chemical composition of a coating polymer with the obtained surficial topographic structures. By tuning various parameters, the toolbox that we offer here, consisting of mussel-inspired polyglycerol building blocks, can be developed further to study surface coatings with well-defined structures from nanoscale to microscale. This can extend the scope of their biomedical applications, e.g. implant surface modification, medical device surface design, and pre-surgery treatment, as well as potential application in regenerative medicine.

2. Results & Discussion

2.1. Mussel-Inspired Polyglycerol Coating Polymers

To explore how the catechol/amine content and the polymer chain conformation affect the coating process and the obtained coating surficial structures, three mussel-inspired polyglycerol coating polymers (MiPGs), i.e., dendritic polyglycerol with 40% catechol and 60% amino groups (dPG40), linear polyglycerol with 80% catechol and 20% amino groups (lPG80), and linear polyglycerol with 40% catechol and 60% amino groups (lPG40) were prepared based on our previous synthesis protocols.[11,27] The dPG40 was obtained by modifying dendritic polyglycerol (M_n = 5180 g mol^{-1}, M_w = 7120 g mol^{-1}, D = 1.37), through amination and amide coupling with 3-(3,4-dihydroxyphenyl)-2-hydroxypropanoic acid (DHHA) under acidic condition, nearly 40% catechol groups functionalization were achieved, with 60% free amines (**Figure 1**a). To prepare the lPG80 and lPG40, poly(allyl glycidyl ether) (PAGE) was first synthesized via ring opening anionic polymerization, followed respectively by thiol-ene and amide coupling reactions (Figure 1b). The degree of catechol grafting densities was controlled by tuning the equivalent relation between DHHA and amino groups from the polymer chain. The obtained lPG40 was characterized by FTIR and NMR (Figure S2, Supporting Information). The adsorption peak at the wavelength of 1518 (cm^{-2}) on the FTIR diagram was assigned to the amide bond, which suggests the successful coupling of catechol groups (Figure S1, Supporting Information). The ^{1}H NMR characteristic peak for the aromatic ring of catechol confirms the successful functionalization. Moreover, the integrals of peaks for catechol and cysteamine allowed us to calculate the functionalization of catechol groups (47% and 83%

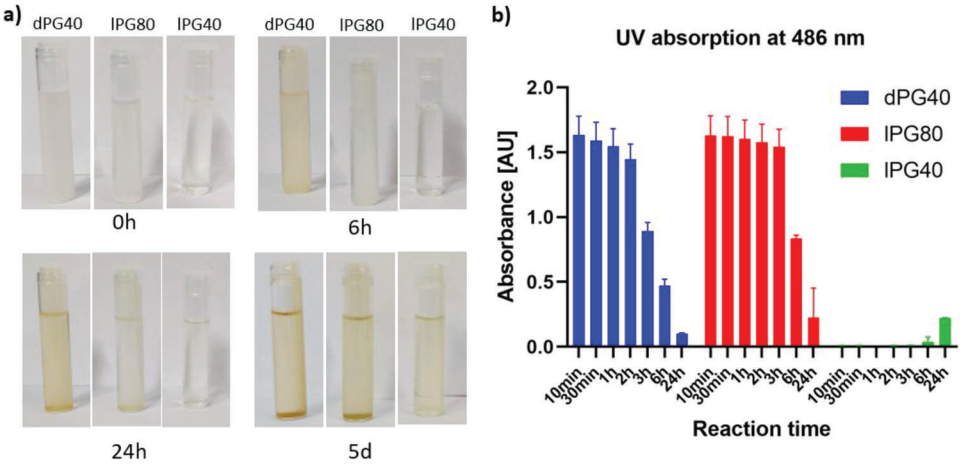

Figure 2. a) Photos of coating solutions after different incubation times (from left to right: dPG40, lPG80, and lPG40). b) UV absorption of coating solutions at wavelength of 486 nm.

of catechol functionalization in lPG40 and lPG80 was achieved, respectively, Figures S2 and S3, Supporting Information).

In mussel adhesion, the catechol group serves as the anchoring domain while amines offer sites for intra- or intermolecular crosslinking. The interplay of catecholic oxidation and amine-induced crosslinking forms a stable and robust network, which contributes to strong adhesion.[28] Under basic conditions, MiPG polymers may undergo vigorous oxidation and covalent crosslinking. Investigation of the reaction rate or coating kinetic guides us to a better understanding of our three MiPG polymers. All three polymers were pre-dissolved in methanol (20 mg polymer in 15 mL, 1.3 mg mL^{-1}), and then 5 mL base aqueous buffer (MOPS buffer, pH = 8.5) was added to form the coating polymer solution (1 mg mL^{-1} in methanol/MOPS buffer solution). The dPG40 and lPG80 solutions immediately turned cloudy after the base buffer addition. However, for lPG40, no obvious change was observed (**Figure 2**a). Meanwhile, due to the exothermic manner of catechol oxidation,[28] dPG40 displayed the most heat release, accompanied by air bubbles in solution. For lPG80 the heat release was less intense, while for lPG40 only extremely small temperature changes were detected. In the coating solution (methanol/MOPS buffer, 3v/1v), the catechol groups underwent immediate oxidation to quinone. Nucleophilic addition then occurred between the amine and quinone, forming quinone-amine adducts. In the meantime, a Schiff-base reaction took place between amine and quinone to yield imine. These reactions contributed to the crosslinking of the polymer.[26,29] The obtained highly crosslinked polymer microgel-like aggregates were insoluble in the coating solution and subsequently precipitated. In the case of dPG40 and lPG80, these aggregates grew larger and then bonded tightly to the bottom of the vials with incubation. After the thorough consumption of polymer, the solution was clarified again, and a thick polymer layer was found at the bottom of the vial (Figure 2). For lPG40, the polymer solution remained clear for days, as expected for this significantly milder reaction. UV–vis spectra were performed to analyze the reactions. The absorption at the wavelength of 486 nm was ascribed to the polymer aggregates formed in the solution. The change in the absorbance at 486 nm allowed us to investigate the reaction kinetics of these coating polymers under base condition. In Figure 2b, both dPG40 and lPG80 showed strong absorption because of the immediate occurrence of the aggregates (≈1.78 AU), while no obvious absorption was observed for lPG40. Besides, a drastic decrease at 3 h for dPG40 (from 1.78 to 0.96 AU) suggests the rapid precipitation of polymer aggregates from solution, indicating a faster reaction rate than lPG80. After 24 h, both dPG40 and lPG80 solution became clear and showed very low UV–vis absorption, while an increase in lPG40 was found (up to 0.22 AU), proving that the slow reaction of lPG40 under the same condition.

2.2. MiPG Coating with Well-Defined Surface Structures

Mussel-inspired coating polymers are well-known as universal coatings that can form stable coating layers on various substrates, such as TiO_2, PS (polystyrene), and glass, via coordinative and/or hydrogen bonding depending on the substrate (Figure 1c).[30] Here we used glass substrates (1 cm × 1 cm), on which MiPG coatings were formed via simple dip-coating method at room temperature.

As mentioned before, insoluble polymer aggregates formed after incubation under basic conditions, then precipitated and attached to the substrate to achieve a coating layer. These aggregates adhered tightly to the surfaces of glass slides via hydrogen bonding. By controlling the coating time, these three different polymers formed coatings with different thickness and topographical features. As seen in **Figure 3**a, a thin and translucent layer was quickly formed on the glass slides, and a yellow and opaque layer was observed with increasing incubation time. Shorter times taken to form a thick opaque coating indicated faster coating kinetic. The transmittance of the resulting coatings was measured by UV–vis spectrometry. A drastic decrease in the transmittance of the dPG40 coating surface was observed within one hour of dip-coating. In comparison, for lPG80 transmittance dropped below 10% after 3 h. No significant decrease was observed for lPG40, even after 48 h (Figure 3b). This result agreed with our observations of the polymer solution and suggests that dPG40 was more reactive and formed a coating more

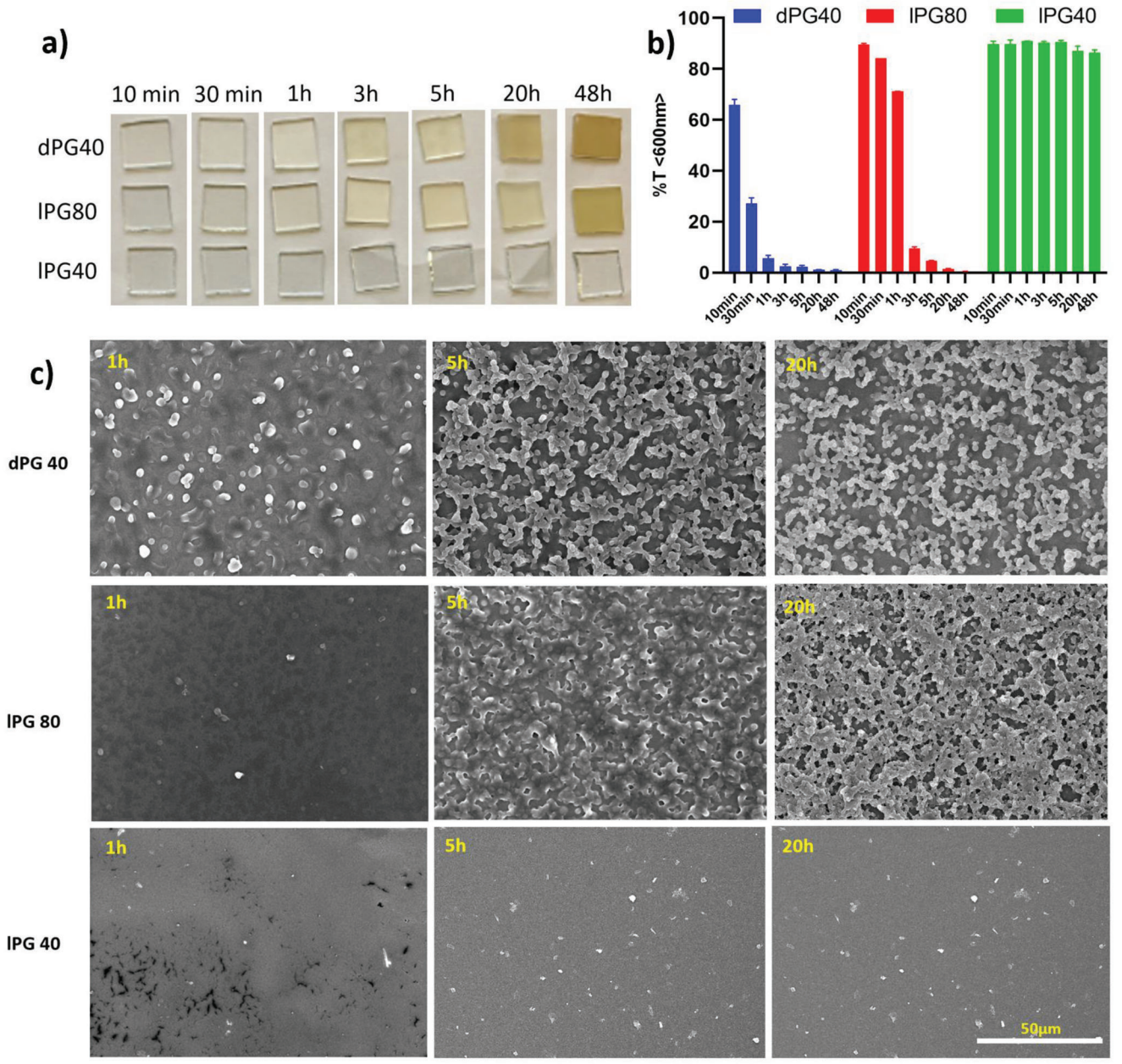

Figure 3. a) Pictures of dPG40, lPG80, and lPG40 coatings on glass substrates with different incubation times. b) Transmittance of dPG40, lPG80, and lPG40 coated glass substrates measured by UV–vis spectrometry. c) SEM images of dPG40, lPG80, and lPG40 coatings with different incubation time. The scale bar indicates 50 µm.

rapidly than the other two polymers. In comparison, lPG80 displayed similar results to dPG40 with a relatively longer incubation time, while lPG40 showed barely any evidence of thick coating layers. The dendritic structure is renowned for its potential to provide a multivalent adhesion system, thus providing multiple sites for crosslinking and greatly enhancing reaction efficiency as compared to the linear structure. On the other hand, owing to the manner of the reaction mechanism, the oxidation of catechol groups is the main factor in determining reaction speed, because only the presence of oxidized catechols can effectively crosslink the quinones and amines. Hence, a higher content of catechol groups results in a faster coating process. Despite the higher catechol content in lPG80, dPG40 still showed a faster coating process. This can be attributed to the linear chain structure of lPG80. In a linear polymer solution, one would expect a greater degree of possible entanglement and a larger hydrodynamic volume, both of which would hinder reactivity during the coating process.

After formation of aggregates in a coating solution, aggregates would accumulate on the substrate, resulting in certain architectures on the coating surfaces. The surface topology is supposedly determined by the size of aggregates and how they come together to form the coating layer. The surface structures of the coatings

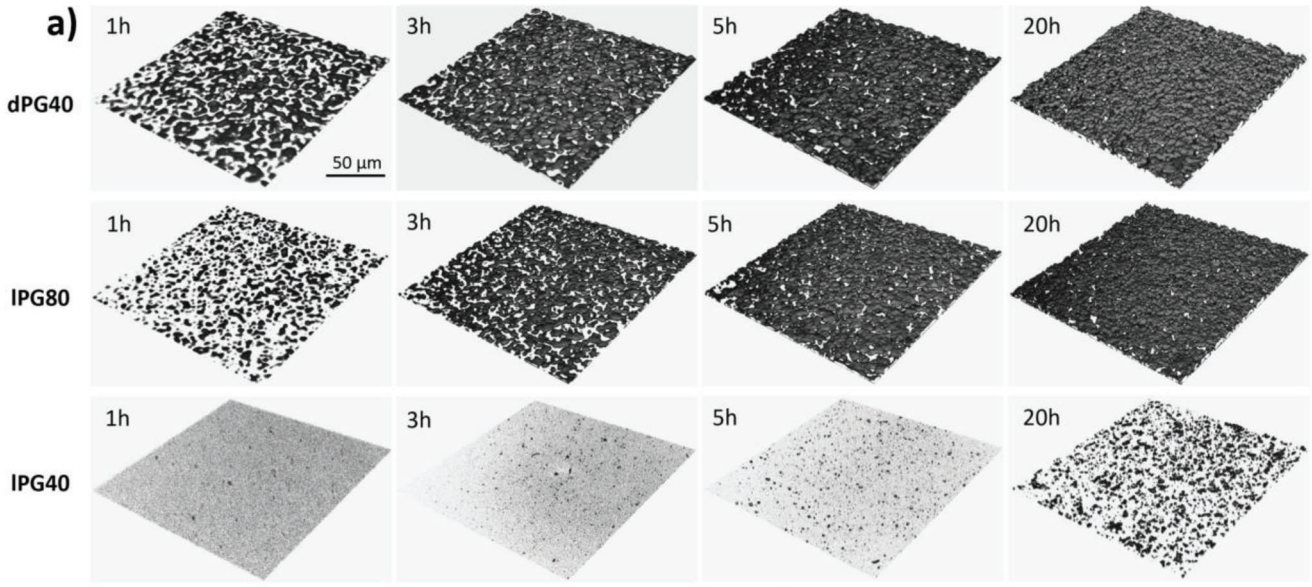

b)

Coating time	Thickness (µm)			Roughness (Rq in µm)		
	dPG40	lPG80	lPG40	dPG40	lPG80	lPG40
3h	4.75 ± 0.39	3.73 ± 0.40	0.55 ± 0.07	1.62 ± 0.12	1.54 ± 0.14	0.02 ± 0.01
5h	5.83 ± 0.42	4.74 ± 0.47	1.00 ± 0.14	1.89 ± 0.23	2.64 ± 0.16	0.04 ± 0.01
20h	7.08 ± 0.61	6.75 ± 0.29	1.87 ± 0.29	2.87 ± 0.18	3.18 ± 0.25	0.32 ± 0.03

Figure 4. a) 3D-model of MiPG coating layer detected by CLSM. b) Summary of the thickness and roughness (Rq, root mean square) of dPG40, lPG80, and lPG40 coating surfaces.

were detected by SEM. As shown in Figure 3c, the biggest aggregates were found in dPG40-coated samples. The size of the generated aggregates decreased from 2.84 ± 0.82 µm (1 h) to 2.41 ± 0.57 µm (5 h), then reached 2.17 ± 0.63 µm (20 h). The decrease in size with incubation time is explained by the consumption of the polymers in solution as the polymer concentration decreases with time. While smaller sizes of aggregates formed on lPG80, which decrease from 1.77 ± 0.33 µm (5 h) to 1.51 ± 0.25 µm (20 h). As results indicated above, dPG40 is the most reactive coating polymer compared with the other two. Under basic conditions, it is prone to a fast oxidation and crosslinking reaction, quickly generating aggregates in the solution, depositing onto the substrate surface and self-growing from the substrate surface. Because of the entanglement polymer conformation, the less reactive lPG40 slowly crosslinked and formed a comparatively smooth monolayer coating with smaller surficial structures.

Due to the detection limitation of AFM (atomic force microscope), it was very challenging to image a surface structure with high roughness (Rq > 1.5 µm).[31] Therefore, confocal laser scanning microscope (CLSM) was used to analyze topographical structures of these coating surfaces. CLSM can be implemented as an alternative to AFM benefiting from the autofluorescent nature of the eumelanin structure on MiPG coating surface.[32] 3D models of the coating layer were reconstructed by z-stacking scanning (Figure S8, Supporting Information). The coating thickness was measured from the z-stacking of the 3D models and the surface roughness was analysed and calculated through ImageJ with the RoughnessCalculation Plugin. The resulting roughness values were presented as root mean square (Rq in µm). As shown in **Figure 4**b, dPG40 yielded thicker coating in a relatively short time (4.75 µm at 3 h to 7.08 µm at 20 h). While lPG80 needed more time to form comparable thickness (3.73 µm at 3 h to 6.75 µm at 20 h) compared to dPG40. Moreover, the dPG40 surfaces were rougher than lPG80 (1.62 µm and 1.54 µm, respectively) due to the faster formation of the coating layer. However, as the coating process continued, the roughness of the lPG80 layer (Rq = 2.64 µm at 5 h) surpassed that of dPG40 (Rq = 1.89 µm), reaching 3.18 µm after 20 h in comparison to and 2.87 µm for dPG40. As discussed before, smaller aggregates are formed when the polymer concentration is lower in lPG80, the piling up of smaller aggregates increased the gap between peaks and valleys the roughness profile, yielding higher roughness parameter value. As for lPG40, the thickness and roughness were difficult to be measured using this method since only very thin layers of polymer films can be formed, causing barely no changes on the glass surface.

Wettability of a surface is dependent not only on the surficial chemical composition but also on the physical structures. Roughness plays an important role in surface static contact angle.[33] In the measurements, although the MiPG polymer is hydrophilic, higher contact angle values were obtained with the increase of the roughness parameters (**Figure 5**). The water contact angle of lPG80 increased from 31° ± 1.7° (10 min) to 52.3° ± 2.3° (5 h). We assume water droplets wetted the surfaces as predicted by

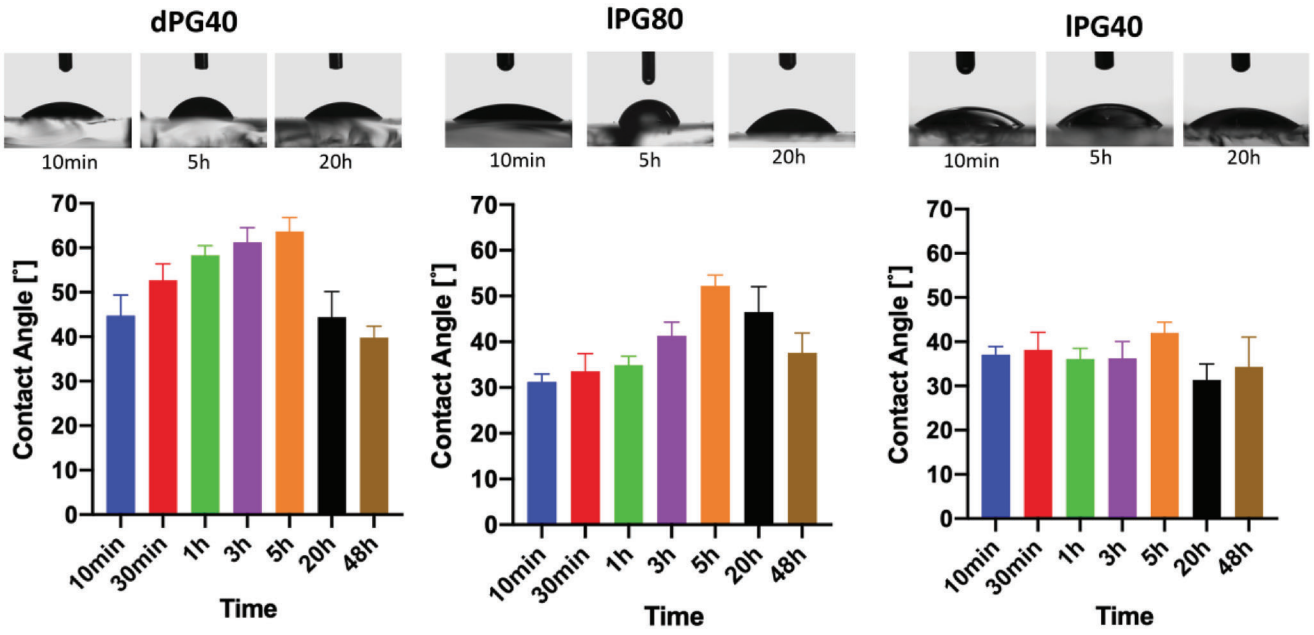

Figure 5. Wettability of dPG40, lPG80, and lPG40 coating surfaces.

the Cassie-Baxter model, where higher roughness contributes to higher hydrophobicity, as more air can be trapped in the grooves during inhomogeneous wetting.[34] However, a decrease in contact angle values was observed in both dPG40 and lPG80 (20 h and 48 h). This can be explained by the fact that after the roughness exceeds a certain value, the grooves become big enough and the water molecules can easily spread within the surficial structures, resulting in lower contact angle values (37.6° ± 4.3° for lPG80, 48 h and 39.8° ± 2.5° for dPG40, 48 h).

XPS was used to characterize the chemical compositions of the MiPG coated surface. In the deconvoluted C-1s spectra, similar chemical compositions were observed for all materials, confirming the successful surface coating with MiPG polymer (**Figure 6**). The chemical composition of the surface coating remained unchanged even after a long period of incubation in the coating solution, demonstrating the stability of this coating surface in aqueous solution. Besides, the chemical compositions of the surface coatings, also the elemental compositions were studied (Figure S7, Supporting Information). The absence of sulphur in dPG40 and the presence of that in lPG80 and lPG40 are explained by the addition of cysteamine during synthesis, some residue of sulphur in dPG40_20 h could be explained by the long incubation time in coating solution which containing MOPS buffer. In contrast to confocal microscopy, where no coating with lPG40 was apparent, the successful chemical functoinalization of glass substrates with lPG40 could be confirmed by XPS, where highly resolved C1s spectrum revealed the chemical composition of the polymer.

2.3. Cell Adhesion on Nanostructured Coated Surfaces

It has been proven that specific nanostructures can enhance cell adhesion as the nanostructured surfaces offer ECM-mimicking morphology, promoting the formation of cellular focal adhesions (FA) and filopodia.[35,11] Controlled interaction between cell and nanostructured substrates enables applications such as control of cell adhesion and detachment, rare cell detection, and regulating stem cell specification.[36,37,9a,b] MiPG polymers have the advantage of forming a well-defined coating with customizable roughness, making it facile to find an optimized structure for cell adhesion.

In this study, we chose human breast cancer cells (MCF-7) as a model cell line to study cell-substrate interaction. As shown in **Figure 7**a and Figure 7b, MCF-7 cells preferentially adhere on the dPG40 surface with roughness at ≈2 µm in Rq, as compared to surfaces with lower or higher surficial roughness values. A similar phenomenon was observed on lPG80 surfaces. However, after optimal surface roughness was reached, substrates with higher roughness impeded the adhesion and spreading of MCF-7 cells. This result was further confirmed by single-cell imaging with SEM. After 3 h of incubation, the adhered cells were fixed and observed. A larger cell spreading area indicated better cell adhesion behavior.[38] The result from SEM was in line with the conclusion we drew from fluorescence microscopy (Figure 7c). A given cell line, due to its particular size and shape, will display a surface-structure-dependent behavior toward the MiPG coated surfaces, which indicates the potential of our coating materials with tunable architectures in biomedical applications.

3. Conclusion

To realize simple and versatile solid surface functionalization with defined nano- and micro-structures for biomedical applications, we designed three mussel-inspired polyglycerol-based coatings with different molecular structures and chemical composition. We then studied their polymer solution, coating processes, and corresponding coated surfaces. It was found that dPG40 can

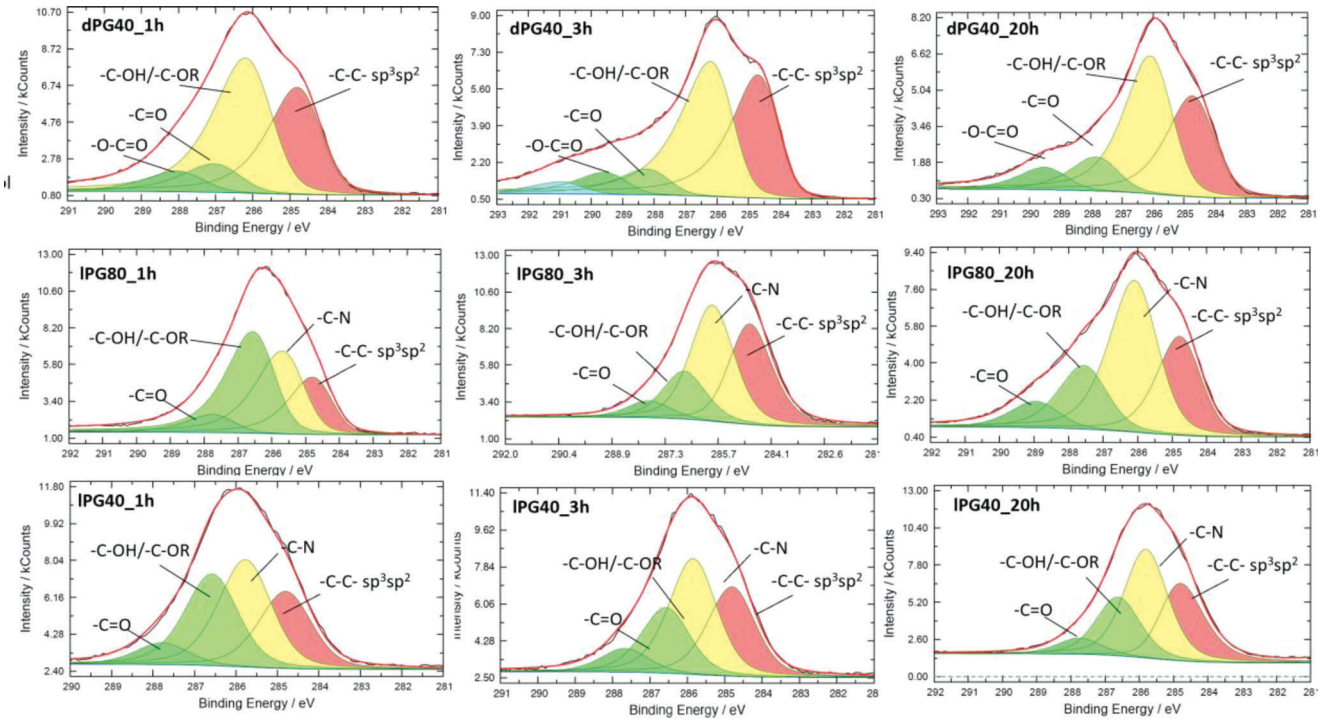

Figure 6. The deconvoluted highly resolved C1s XP spectra of the resulting dPG40, lPG80, and lPG40 coating surfaces.

achieve effective thick coating within one hour despite lower catecholic content in its polymeric chain, yielding a robust, stable hydrogel-like coating layer with a thickness of up to 7 microns. In comparison, the linear structure of lPG80 slowed the reaction due to molecular chain entanglements and a larger hydrodynamic diameter. This decelerated coating process made the resultant coating more controllable than dPG40. Owing to its slower coating process, lPG80 can form coatings with a wider range of roughness (1.54 – 3.18 µm, Rq). This type of coating polymer is therefore especially suitable for fabricating nano and micro-structured surfaces and for application to cell study. Last but not least, although lPG40 could not easily form a measurably thick coating layer, monolayer functionalization was confirmed by XPS. Suggested applications for lPG40 might therefore include only chemical functionalization for further modification, rather than topographical alternation. We investigated the versatility of mussel-inspired polyglycerol coating and demonstrated examples of biological application, and the potential of this type of coating polymer can be suitable for cellular biointerfaces.

4. Experimental Section

Materials and Methods: All chemicals and solvents were used directly without any further purification unless pointed out individually. Dialysis was done in benzoylated cellulose tubes (molecular weight cut-off 2000 g mol^{-1}, Sigma-Aldrich). ^{1}H-NMR spectra were recorded on a Bruker AC 400 under 400 MHz. Analytes were dissolved corresponding deuterated solvents at concentration of ≈20 mg mL^{-1}. Gel permeation chromatography (GPC) measurements were performed on Agilent 1250 series instrument. Molecular weight and distribution were determined by the calibration with standards.

Synthesis of Mussel-Inspired Polyglycerol 40 (dPG40): Dendritic polymer was synthesized according to previous protocol with some modifications.[27a] In brief, dendritic polyglycerol (dPG-OH, M_n = 3816 g mol^{-1}, M_w = 5813 g mol^{-1}, D = 1.52) was functionalized through mesylation, azidation, and reduction. Unlike the previous reported method, where the catechol groups were protected by acetal then deprotected after coupling,[27a] the process was simplified by directly amide coupling with amine and 3-(3,4-dihydroxyphenyl)-2-hydroxypropanoic acid (DHHA) under acidic condition (2-(N-morpholino)ethanesulfonic acid buffer, pH = 5). ^{1}H-NMR (400 MHz, Methanol-d3) δ = 6.65 – 6.46 (m, Ar), 4.02 – 3.05 (m, PG-backbone), 2.72 (m, -COCH$_2$CH$_2$C-), 2.41 (m, -COCH$_2$CH$_2$-).

Synthesis of Poly(allyl glycidyl ether) (PAGE): The PAGE was synthesized through anionic polymerization reaction under argon atmosphere and exclusion of moisture. A Schlenk flask was completely dried, then tetra-n-octylammonium bromide (NOc_4Br 1 g, 1.92 mmol) was added to the flask and dried at in 120 °C for 3 h under vacuum to remove the trace of water. After cooling down to room temperature, dry toluene (30 mL) was added to dissolve the initiator. Afterwards, allyl glycidyl ether (10 mL, 84 mmol) was added, followed by the slow addition of catalyst triisobutylaluminum (6.97 mL, 7.6 mmol) under 0 °C with ice/water bath and then the mixture was stirred overnight. 1 mL of H_2O was added to quench the reaction. The solvent was dried with sodium sulfate then evaporated by rotary distillation. Later diethylene ether was added to precipitate the initiator residues and catalyst and the solvent was removed by evaporation. Further purification was performed by dialysis in dichloromethane (DCM) for 2 days. M_n = 5796 g mol^{-1} ^{1}H-NMR (400 MHz, Chloroform-d) δ = 5.98 – 5.77 (1H, CH$_2$-O-CH$_2$-CH = CH$_2$), 5.32 – 5.05 (2H, CH$_2$-O-CH$_2$-CH = CH$_2$), 3.97 (2H, CH$_2$-O-CH$_2$-CH = CH$_2$), 3.77 – 3.34 (7H, PG-backbone). IR: ν (cm^{-1}) = 3357, 2871, 2101, 1646, 1456, 1350, 1264, 1066, 921, 875.

Thiol-Ene Reaction of PAGE: PAGE was dissolved in THF/MeOH (1:1). Then cysteamine hydrochloride (4 g, 35 mmol, 4 eq. to allyl groups) and 2-2-dimethoxy-2-phenylacetophenone (Irgacure 651, 0.045 g, 2% eqv. to allyl

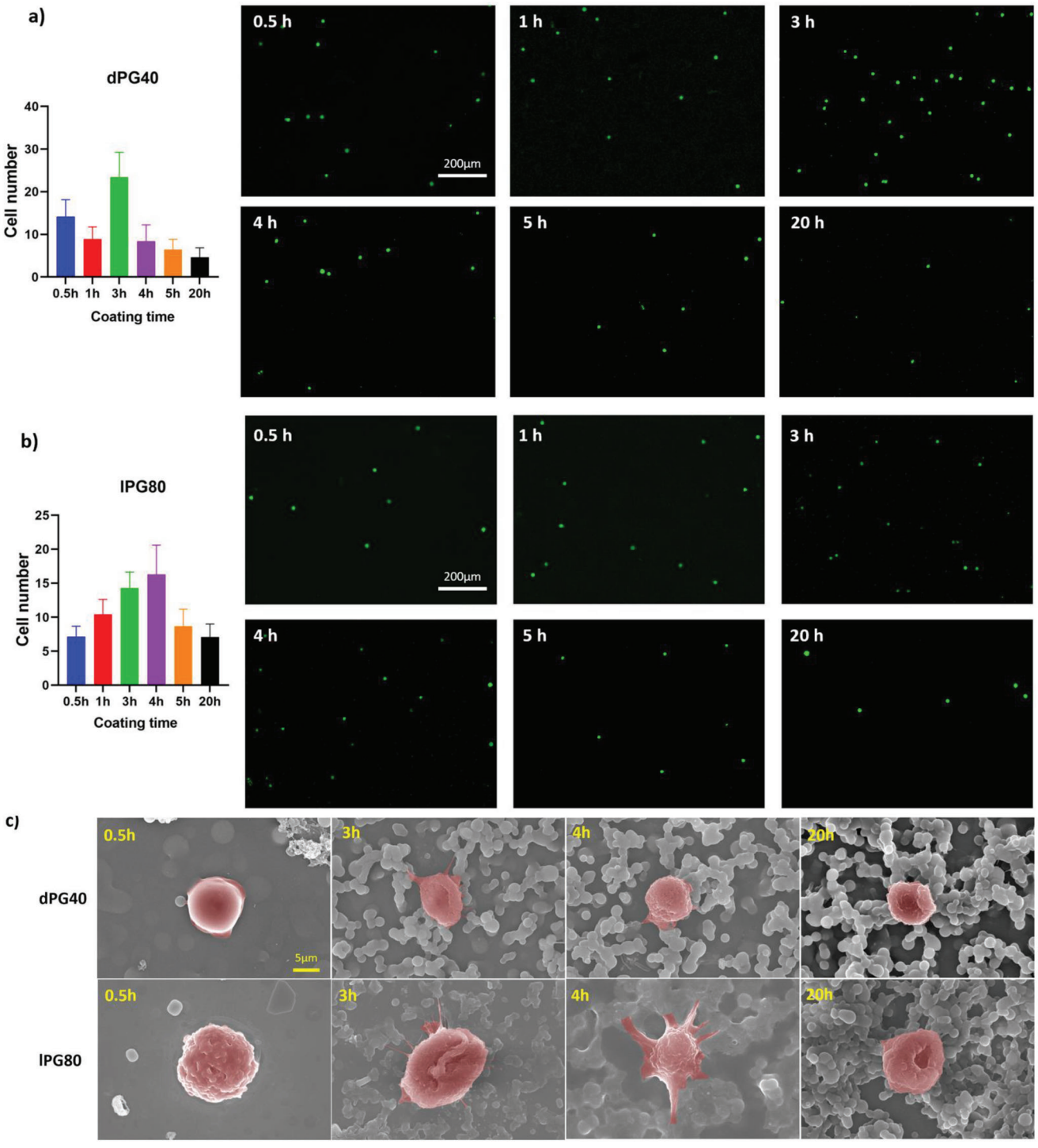

Figure 7. Cell adhesion on MiPG coating surfaces. a) Cells spiked on dPG40 surface; b) Cells spiked on IPG80 surface. MCF-7 cells were spiked and incubated for 3 h before washing with PBS buffer. The remaining stained cells were counted with ImageJ. c) Single-cell morphology characterized by SEM, with larger cell spreading area indicating better cell-substrate interaction.

groups) were added to the mixture. The reaction was carried out under UV radiation (≈1.2 mW cm^{-2}, $\lambda = 365$ nm) at room temperature. The reaction was monitored by ^{1}H-NMR and finished in around 10 hours. Afterwards, the product was purified by dialysis in methanol.

^{1}H-NMR (400 MHz, Deuterium Oxide) δ = 3.87 – 3.49 (8H, PG-backbone), 3.24 (2H, CH_2-S-CH_2-CH_2-N), 2.88 (2H, CH_2-S-CH_2-CH_2-N), 2.68 (2H, CH_2-O-CH_2-CH_2-CH_2-S), 1.91 (2H, CH_2-O-CH_2-CH_2-CH_2-S). IR: ν (cm^{-1}) = 3410, 2862, 2008, 1599, 1479, 1374, 1261, 1108, 932, 887.

Synthesis of Mussel-Inspired Linear Polyglycerol 40 and 80 (lPG40 and lPG80): The catecholic coating polymers were prepared by coupling amino groups from polymer and carboxyl groups from 3,4-dihydroxyhydrocinnamic acid (DHHA). Polymer and 1-Ethyl-3-(3-dimethylaminopropyl) carbodiimide hydrochloride (EDCI, 6 eq. to amino groups) were dissolved into pH 5 MES buffer/methanol (1/1, v/v) mixture solvent. Afterwards, 3,4-dihdroxyhydrocinnamic acid (1.2 eq. to amino groups) was added into the mixture and gently stirred overnight at room temperature. Purification was conducted by dialysis in methanol. ^{1}H-NMR (400 MHz, Methanol-d4) δ = 6.73 – 6.45 (1H, Ar-H), 3.83 – 3.38 (10H, PG-backbone), 3.01 – 2.69 (3H, S-CH_2-CH_2-N), 2.68 – 2.46 (3H, O-CH_2-CH_2-CH_2-S), 1.94-1.66 (2H, O-CH_2-CH_2-CH_2-S). IR: ν (cm^{-1}) = 3133, 2922, 1666, 1602, 1518, 1441,1281, 952, 821

Coating Preparation: Freshly cleaned glass slides were immersed in polymer solution (1 mg mL^{-1} in MeOH/3-(N-morpholino)propanesulfonic acid (MOPS) buffer (pH = 8.5), 3v/1v) for pre-set time points. Afterwards, slides were thoroughly rinsed with methanol, Milli Q water, then dried with nitrogen gas flow. All the slides were further dried in oven (60 °C) overnight before use.

UV–Vis Absorption and Transmission: UV–vis absorption was conducted on Agilent Cary 8454 UV-vis spectrometer, using half-micro quartz cuvettes. Polymers were dissolved in methanol at the concentration of 1 mg mL^{-1}. Upon the addition of MOPS buffer (pH = 8.5), samples were measured at the different time point (10 min, 30 min, 1 h, 2 h, and 3 h, respectively). Methanol/MOPS mixture was employed as background. UV-transmission of the polymer coated slides was measured on Agilent Cary 854 UV–vis spectrometer. Transmittance at the wavelength of 600 nm was used for data analysis.

Scanning Electron Microscopy (SEM): All pre-dried samples were sputtered with a thin layer of gold nanoparticles (≈8–10 nm) under high vacuum using sputter coater (Emscope SC 500, Quorum Technologies, UK). Surface morphology or single cell on substrates were investigated with scanning electron microscope (Hitachi SU8030, Japan, at high voltage of 15 kV, with working distance of 8.3 mm).

Single Cell Imaging with SEM: Spiked cells were incubated for 3 h in RPMI 1640 medium, then gently rinsed with DPBS. Afterwards, cells were fixed with glutaraldehyde solution (2.5 wt.% in DPBS) for 1 h at room temperature, followed by dehydration with ethanol/DPBS gradient solution (30/70, 50/50, 70/30, 90/10, 95/5, 100/0, v/v, 30 min for each time). Critical-point dry was done by Hexamethyldisilazane (HMDS)/ethanol solution (50/50, 100/0, v/v, 30 min for each time). Samples were dried in well-ventilated hood overnight at room temperature before measured with SEM.

Confocal Laser Scanning Microscopy (CLSM): Coated substrates were put on microscope cover glasses (bottom side up, fixed with glycerine), then imaged with confocal laser scanning microscope (Leica SP8). The surface roughness of the coatings was analysed and calculated by ImageJ.

Water Contact Angle (WCA): Water contact angle measurements were carried out on a contact angle goniometer (DataPhysics Instruments, Germany) with sessile drop method. Mean values of several measurements of each sample were taken.

X-Ray Photoelectron Spectroscopy: X-ray photoelectron spectroscopy (XPS) spectra were recorded on a Kratos (Manchester, UKAxis Ultra DLD spectrometer), equipped with a monochromatic Al Kα X-ray source. The spectra were measured in normal emission, and a source-to-sample angle 60° was used. All spectra were recorded utilizing the fixed analyzer transmission (FAT) mode. The binding energy scale of the instrument was calibrated, following a technical procedure provided by Kratos Analytical Ltd (calibration was performed according to ISO 15 472). The spectra were recorded utilizing the instrument's slot and hybrid lens modes. An analysis area of ≈300 µm x 700 µm was investigated; charge neutralization was applied. For quantification, the survey spectra were measured with a pass energy of 80 electron Volt (eV), and the spectra were quantified utilizing the empirical sensitivity factors that were provided by KRATOS (the sensitivity factors were corrected with the transmission function of the spectrometer). The high-resolution XPS spectra were measured with a pass energy of 20 eV, and the respective data were processed using UNIFIT 2020 spectrum processing software. For peak fitting, a Shirley background and a Gaussian/Lorentzian sum function were applied. If not denoted otherwise, the L-G mixing component was set to 0.35 for all peaks. All binding energies were calibrated to the signal observed for the C sp^2/sp^3 component (observed at 284.8 eV).

Cell Culture and Cell Adhesion Analysis: Human breast cancer cell lines (MCF7) were obtained from the American Type Culture Collection (ATCC). Roswell Park Memorial Institute RPMI-1640 culture medium (Gibco) was supplemented with 10% (v/v) fetal bovine serum (FBS) (Gibco) and 1% (v/v) of penicillin-streptomycin solution (Gibco). All the cancer cell lines were cultured at 37 °C with 5% CO_2 in culture flask.

MCF-7 cells were first dissociated by trypsin solution (Gibco) for 2 min. Then the cells were pre-stained with CellTrace™ Violet dye (Thermo Fisher Scientific, Waltham, MA, USA) for 20 min according to standard protocol from the manufacturer. Stained cells were spiked in serum-free RPMI-1640 medium with a concentration of 5000 cells mL^{-1}. Samples were incubated in 1 mL of prepared cell suspension for 3 h at 37 °C. Afterwards, all samples were gently rinsed with DPBS for 3 times to remove the excess cells then observed and photographed under fluorescence microscope (Zeiss Axio Observer Z1).

Supporting Information

Supporting Information is available from the Wiley Online Library or from the author.

Acknowledgements

The authors acknowledge the financial support of Dahlem research school (DRS) and Collaborative Research Center "Dynamic Hydrogels at Biological Interfaces"(CRC 1449) funded by the Deutsche Forschungsgemeinschaft (DFG, German Research Foundation) – Project ID 431232613 – SFB 1449. The authors would like to thank Cathleen Hudziak for providing the starting polymer dendritic polyglycerol (dPG) and Core Facility BioSupraMol (Freie Universität Berlin, Germany) for the support in SEM and CLSM measurements. Yannic Kerkhoff is thanked for offering help with ImageJ analysis of confocal 3D image. The authors also thank Benjamin Allen for polishing the manuscript. The authors want to thank Gary Chinga and Bob Dougherty for the development of RoughnessCalculation Plugin.

Conflict of Interest

The authors declare no conflict of interest.

Data Availability Statement

The data that support the findings of this study are available in the Supporting Information of this article.

Keywords

biointerfaces, cell adhesion, mussel-inspired polyglycerols, surface functionalization

Received: February 24, 2023
Revised: April 25, 2023
Published online: May 28, 2023

[1] J.-O. Carlsson, P. M. Martin, in *Handbook of Deposition Technologies for films and coatings*, Elsevier, New York **2010**, p. 314.
[2] J. C. Love, L. A. Estroff, J. K. Kriebel, R. G. Nuzzo, G. M. Whitesides, *Chem. Rev.* **2005**, *105*, 1103.
[3] N. Sahu, B. Parija, S. Panigrahi, *Indian J. Phys.* **2009**, *83*, 493.
[4] S. Minko, in *Polymer surfaces and interfaces*, Springer, New York **2008**, p. 215.
[5] E. Luong-Van, I. Rodriguez, H. Y. Low, N. Elmouelhi, B. Lowenhaupt, S. Natarajan, C. T. Lim, R. Prajapati, M. Vyakarnam, K. Cooper, *J. Mater. Res.* **2013**, *28*, 165.
[6] R. Smeets, B. Stadlinger, F. Schwarz, B. Beck-Broichsitter, O. Jung, C. Precht, F. Kloss, A. Gröbe, M. Heiland, T. Ebker, *Biomed Res. Int.* **2016**, *2016*, 3943481.
[7] S. B. Goodman, Z. Yao, M. Keeney, F. Yang, *Biomaterials* **2013**, *34*, 3174.
[8] D. Choudhury, M. Vrbka, A. B. Mamat, I. Stavness, C. K. Roy, R. Mootanah, I. Krupka, *J. Mech. Behav. Biomed. Mater.* **2017**, *72*, 192.
[9] a) J. Dong, J. F. Chen, M. Smalley, M. Zhao, Z. Ke, Y. Zhu, H. R. Tseng, *Adv. Mater.* **2020**, *32*, 1903663; b) A. Singh, M. Ferri, M. Tamplenizza, F. Borghi, G. Divitini, C. Ducati, C. Lenardi, C. Piazzoni, M. Merlini, A. Podestà, *Nanotechnology* **2012**, *23*, 475101; c) M. J. Dalby, N. Gadegaard, R. O. Oreffo, *Nat. Mater.* **2014**, *13*, 558; d) J. Li, X. Jiang, H. Li, M. Gelinsky, Z. Gu, *Adv. Mater.* **2021**, *33*, 2004172.
[10] Y. Hou, W. Xie, L. Yu, L. C. Camacho, C. Nie, M. Zhang, R. Haag, Q. Wei, *Small* **2020**, *16*, 1905422.
[11] L. Yu, P. Tang, C. Nie, Y. Hou, R. Haag, *Adv. Healthcare Mater.* **2021**, *10*, 2002202.
[12] D. Qin, Y. Xia, G. M. Whitesides, *Nat. Protoc.* **2010**, *5*, 491.
[13] Y. Lei, S. Yang, M. Wu, G. Wilde, *Chem. Soc. Rev.* **2011**, *40*, 1247.
[14] K. Q. Peng, Y. J. Yan, S. P. Gao, J. Zhu, *Adv. Mater.* **2002**, *14*, 1164.
[15] B. Sun, Y. Long, H. Zhang, M. Li, J. Duvail, X. Jiang, H. Yin, *Prog. Polym. Sci.* **2014**, *39*, 862.
[16] Q. Wei, R. Haag, *Mater. Horiz.* **2015**, *2*, 567.
[17] N. Sun, X. Li, Z. Wang, R. Zhang, J. Wang, K. Wang, R. Pei, *ACS Appl. Mater. Interfaces* **2016**, *8*, 12638.
[18] S. Hou, J.-F. Chen, M. Song, Y. Zhu, Y. J. Jan, S. H. Chen, T.-H. Weng, D.-A. Ling, S.-F. Chen, T. Ro, *ACS Nano* **2017**, *11*, 8167.
[19] L. Zhao, Y. T. Lu, F. Li, K. Wu, S. Hou, J. Yu, Q. Shen, D. Wu, M. Song, W. H. OuYang, *Adv. Mater.* **2013**, *25*, 2897.
[20] H. G. Silverman, F. F. Roberto, *Mar. Biotechnol.* **2007**, *9*, 661.
[21] H. Lee, S. M. Dellatore, W. M. Miller, P. B. Messersmith, *Science* **2007**, *318*, 426.
[22] M. Lee, S. H. Lee, I. K. Oh, H. Lee, *Small* **2017**, *13*, 1600443.
[23] Q. Wei, F. Zhang, J. Li, B. Li, C. Zhao, *Polym. Chem.* **2010**, *1*, 1430.
[24] Y. Tan, W. Deng, Y. Li, Z. Huang, Y. Meng, Q. Xie, M. Ma, S. Yao, *J. Phys. Chem. B* **2010**, *114*, 5016.
[25] W. Sheng, B. Li, X. Wang, B. Dai, B. Yu, X. Jia, F. Zhou, *Chem. Sci.* **2015**, *6*, 2068.
[26] J. Yang, C. Stuart, *Chem Soc Rev* **2014**, *43*, 8271.
[27] a) Q. Wei, K. Achazi, H. Liebe, A. Schulz, P. L. M. Noeske, I. Grunwald, R. Haag, *Angew. Chem., Int. Ed.* **2014**, *53*, 11650; b) C. Schlaich, L. C. Camacho, L. Yu, K. Achazi, Q. Wei, R. Haag, *ACS Appl. Mater. Interfaces* **2016**, *8*, 29117.
[28] H. Lee, N. F. Scherer, P. B. Messersmith, *Proc. Natl. Acad. Sci. USA* **2006**, *103*, 12999.
[29] B. K. Ahn, *J. Am. Chem. Soc.* **2017**, *139*, 10166.
[30] M. l. W. Kulka, I. S. Donskyi, N. Wurzler, D. Salz, O. z. Özcan, W. E. Unger, R. Haag, *ACS Appl Bio Mater* **2019**, *2*, 5749.
[31] S. S. Ray, *Clay-containing polymer nanocomposites* **2013**, *39*, 1112.
[32] P. Meredith, B. J. Powell, J. Riesz, S. P. Nighswander-Rempel, M. R. Pederson, E. G. Moore, *Soft Matter* **2006**, *2*, 37.
[33] R. N. Wenzel, *J. Phys. Chem.* **1949**, *53*, 1466.
[34] S. Giljean, M. Bigerelle, K. Anselme, H. Haidara, *Appl. Surf. Sci.* **2011**, *257*, 9631.
[35] L. Wang, W. Asghar, U. Demirci, Y. Wan, *Nano Today* **2013**, *8*, 374.
[36] W. Zhou, X. Zhong, X. Wu, L. Yuan, Z. Zhao, H. Wang, Y. Xia, Y. Feng, J. He, W. Chen, *Surf. Coat. Technol.* **2006**, *200*, 6155.
[37] W. Chen, S. Weng, F. Zhang, S. Allen, X. Li, L. Bao, R. H. Lam, J. A. Macoska, S. D. Merajver, J. Fu, *ACS Nano* **2013**, *7*, 566.
[38] K. Anselme, L. Ploux, A. Ponche, *J. Adhes. Sci. Technol.* **2010**, *24*, 831.